

Watertable Fluctuations in a Sandy Ocean Beach

B. Raubenheimer¹, R.T. Guza¹, and Steve Elgar²

Abstract

Fluctuations of the watertable level within a fine-grained beach were observed for 2 months in Fall 1996. The magnitude of fluctuations at diurnal and semi-diurnal frequencies decayed rapidly inland, but fluctuations at spring-neap frequencies remained significant nearly 100 m inland of the mean shoreline location. During two storms that coincided with spring tides, overtopping and ponding of water behind the berm resulted in increased watertable levels that persisted for several days. Beach erosion during the second storm resulted in landward displacement of the shoreline location, and subsequent watertable fluctuations also extended farther inland. Numerical solutions of the nonlinear Boussinesq equation, with the seaward boundary condition given by the observed shoreline location, agree well with the observations. The landward attenuation and phase shifting of tidal watertable fluctuations are predicted well, as is the location of the seepage face.

Introduction

Beach watertable levels are believed to affect swash zone fluid motions (e.g., Packwood, 1983) and sediment transport (e.g., Grant, 1948; Duncan, 1964; Eliot and Clarke, 1988). Tidal watertable fluctuations in shallow (relative to the wavelength of the fluctuations) aquifers are often modeled with the nonlinear Boussinesq equation

$$\frac{\partial \eta}{\partial t} = \frac{K}{N} \frac{\partial}{\partial x} \left((D + \eta) \frac{\partial \eta}{\partial x} \right) \quad (1)$$

where t is time, x is the cross-shore coordinate, η and D are, respectively, the deviation of the watertable elevation and the depth of the impermeable stratum relative to mean sea level, K is the hydraulic conductivity in the saturated beach, and N is the effective porosity. The observed asymmetry (the beach fills more rapidly than it drains) and

¹Scripps Inst. Oceanography, 9500 Gilman Dr., La Jolla, CA, 92093-0209, britt@coast.ucsd.edu

²E ECS 2752, Washington State University, Pullman, WA, 99164-2752

overheight (the mean inland watertable elevation is higher than mean sea-level) of tidal watertable fluctuations (e.g., Emery and Foster, 1948; Harrison et al., 1971; Waddell, 1976; Lanyon et al., 1982) that result from the moving intersection of the waterline with the sloping beach are predicted qualitatively by analytical solutions of (1) for small tidal excursions on a planar beach (Nielsen, 1991). However, the tidal overheight is underpredicted, possibly because the model neglects the effects of the seepage face, the decoupling of the watertable and offshore water level that occurs on fine-grained beaches near low tide (Turner, 1993). Comparisons of numerical solutions of (1) with watertable fluctuations observed over one or two tidal cycles suggest the seepage face and wave-driven setup at the shoreline are important to watertable fluctuations (Kang and Nielsen, 1996; Baird et al., 1998).

Here, watertable fluctuations observed along a densely instrumented cross-shore transect are used to extend the previous studies. The 2 months of observations span several spring-neap tidal cycles and include a storm that modified the beach profile. Comparisons of the observations with numerical solutions of (1) are used to identify processes important to watertable fluctuations and the seepage face location.

Observations

Waves, runup, tides, and watertable fluctuations were sampled nearly continuously at 2 Hz for two months during Fall 1996 at Torrey Pines Beach, CA (Figure 1). Surf zone waves and runup were measured with 16 pressure sensors located near the sand surface, and watertable fluctuations were measured with 22 buried pressure sensors. Runup and watertable sensors were stacked vertically to estimate vertical infiltration and to detect capillary effects. Beach profiles landward of about 2-m water depth were measured daily throughout September and October and approximately every other day during November. Other than erosion during a storm in late October (Figure 1), foreshore profile changes were small (< 10 cm). At the beginning, middle, and end of the experiment the profile was measured to about 5-m water depth. Offshore wave heights measured in 10-m water depth about 35 km north of the experiment site ranged from 40 to 330 cm and peak periods ranged from 5 to 20 s (Figure 2B). These offshore observations agreed well with measurements made at Torrey Pines Beach in about 3.5-m water depth at cross-shore distance 165 m (Figure 1), except during the storms when the shallower sensor was in the surf zone. Rainfall of 0.76 and 1.62 cm were recorded on Oct 26 and 30, respectively.

At fifteen locations between cross-shore distances 10 and 100 m, 8-m deep holes were drilled to collect sediment cores and to determine the beach stratigraphy. Sieve analysis was conducted on eleven cores to determine grain sizes, and five cores were used to determine porosity. Hydraulic conductivity was estimated from pumping tests (Bouwer and Rice, 1976) conducted at cross-shore distances 60 and 91 m. The beach is composed of approximately 2 to 4 m of uniform fine to medium sand with traces of silt ($d_{50} \approx 0.23$ mm, porosity $\approx 37\%$, and hydraulic conductivity ≈ 0.07 cm/s) overlying about 1 m of Scripps formation composed of dense, silty fine sand with traces of gravel ($d_{50} \approx 0.15$ mm, porosity $\approx 33\%$, and hydraulic conductivity ≈ 0.03 cm/s) on top of low permeability Ardath Shale ($d_{50} \approx 0.004$ mm, porosity $\approx 32\%$, and hydraulic conductivity ≈ 0.0005 cm/s). All pressure sensors were located above the Scripps formation and are identified by their distance (in m) inland from the mean shoreline location, defined as the intersection of the beach profile and mean

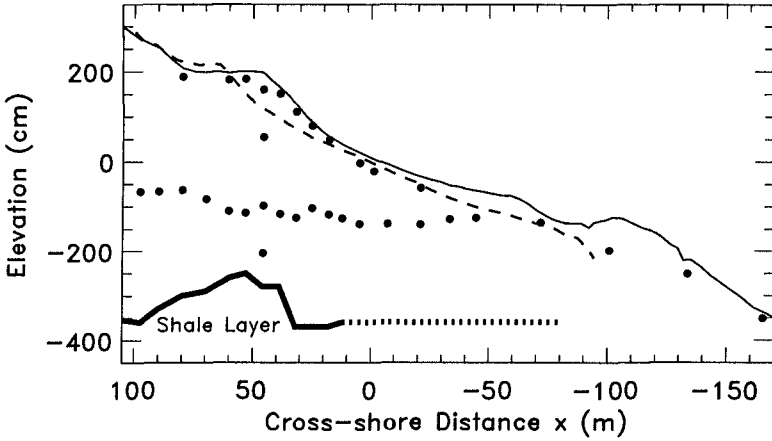


Figure 1: Pressure sensor locations (solid circles) and beach profiles measured at Torrey Pines Beach before (thin solid curve) and after (thin dashed curve) a storm on Oct 25. The thick solid and dotted curves at the bottom of the figure represent the measured upper surface of the Ardash Shale and the (unmeasured) offshore shale position used in the numerical model, respectively.

sea level (e.g., p098 is located at 98 m).

The observed mean watertable levels usually increased in the landward direction, suggesting that water usually flowed toward the ocean (Figure 2A). Tidal watertable and offshore fluctuations were dominated by waves with 25 and 12 hr periods (Figure 3). Similar to previous observations (e.g., Emery and Foster, 1948; Harrison et al., 1971; Waddell, 1976; Lanyon et al., 1982), tidal watertable fluctuations were asymmetrical in time (not shown), and decreased rapidly in magnitude in the landward direction (Figures 2 and 3). Offshore tidal amplitudes ranged from about 0.5 m during neap tides to 1 m during spring tides (Figure 2C), whereas watertable fluctuation amplitudes at cross-shore distance 60 m were usually less than about 10 cm (Figure 2A). At the most landward sensor, 98 m inland of the mean shoreline, diurnal and semi-diurnal tidal fluctuations were strongly damped, but fluctuations at the frequency of the spring-neap tidal cycle remained significant (Figure 2A). Spring-neap watertable fluctuations have not been observed previously, possibly because most observations spanned only a few days. For similar offshore tidal fluctuations and wave heights, watertable fluctuations near the berm were smaller in September than in November (Figure 2) because beach erosion (Figure 1) on Oct 26 reduced the distance from the berm to the mean shoreline.

Wind waves had a significant effect on the observed watertable fluctuations. During two storms (offshore wave heights greater than about 130 cm) that occurred during spring tides (Oct 15 and Oct 25 in Figure 2) runup overtopped the berm, resulting in large (up to 70 cm) increases in the berm watertable level. High watertable levels persisted for several days after each storm. However, tidal levels modulated the effect of storm waves on watertable fluctuations. For instance, although offshore wave heights exceeded 130 cm during the neap tides (Figure 2, Oct 20), berm overtopping did not occur and the berm watertable response was small.

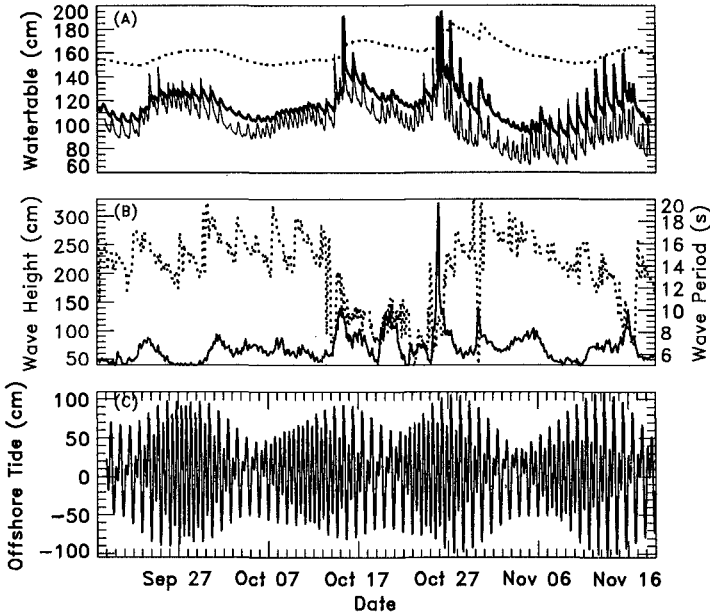


Figure 2: Observed (A) 10-min averaged watertable levels at cross-shore locations 98 (dotted curve), 60 (thick solid curve), and 46 m (thin solid curve) inland of the mean shoreline, (B) offshore hourly significant wave heights (solid curve) and peak wave periods (dotted curve), and (C) 34-min averaged offshore sea-surface levels versus time.

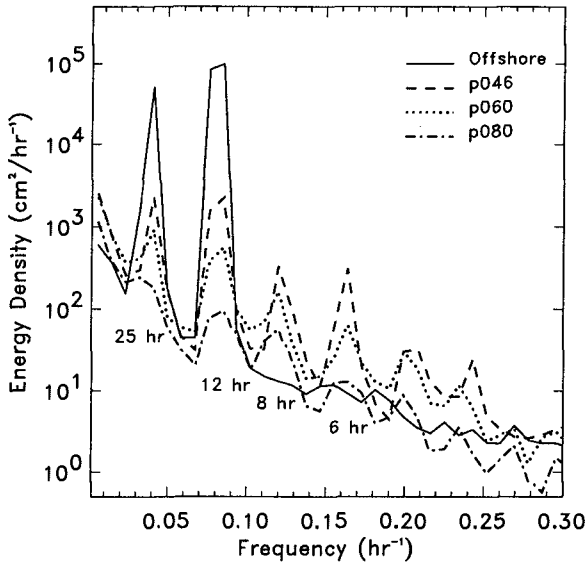


Figure 3: Energy spectra (24 dof) of offshore water-level (solid curve) and watertable fluctuations at 46 (dashed curve), 60 (dotted curve), and 80 m (dash-dot curve) inland of the mean shoreline.

Numerical Model

The observations are compared with numerical solutions of the nonlinear Boussinesq equation (1). A no flow bottom boundary condition is imposed at the top of the Ardath Shale (Figure 1), which is assumed to be horizontal both landward and seaward of the measured positions. Above the impermeable boundary, the beach material is assumed homogeneous and isotropic, with an average hydraulic conductivity K of 0.07 cm/s. The effective porosity N , determined using a least squares fit of the predictions to the observations, is 0.215. The model is initialized with the watertable level observed at the start of the experiment. Initial levels inland of the most landward sensor are estimated using a natural cubic spline extrapolation. The location of the inland boundary (250 m landward of the mean shoreline) was determined iteratively to ensure it was sufficiently far onshore that predicted watertable fluctuations were negligible. In the results presented below, a constant head (Dirichlet) condition is imposed at the inland boundary of the model domain. The model results are sensitive to the ratio K/N and to the aquifer thickness D , but are insensitive to the inland boundary condition.

The beach is assumed to be saturated at, and offshore of, the model seaward boundary, which is given by the shoreline location (e.g., the beach-ocean intersection). The moving locations of the shoreline and the watertable outcrop at the sand surface were estimated using water levels observed with the closely spaced foreshore sensors and measured beach profiles. The cross-shore structure of the mean water level was estimated by fitting a cubic spline to 10-min averaged observations at all sensors. Sand levels at each time step were determined by fitting a cubic spline to the measured beach profiles. The shoreline location was defined as the most seaward location where the water depth above the beach profile was less than a small number δ_s . The watertable outcrop location was estimated from the observations as the most landward position where the measured water level was less than δ_w below sand level. Owing to errors of a few cm in the measured mean pressure and beach profiles, nonzero values are used for δ_s and δ_w . The results shown below correspond to $\delta_s = \delta_w = 2$ cm and are not sensitive to values of δ_s and δ_w between 1 and 5 cm. Following van Gent (1994) and Baird et al. (1996), when the predicted watertable level exceeds the sand level within the model domain (landward of the shoreline), the watertable is reset to sand level and the excess water is assumed to be run-off.

The Boussinesq equation (1) is based on the assumption that horizontal flows u are much larger than the vertical flows w . The flow through saturated sand was estimated using observed gradients of hydraulic head ($p_w/\rho g + z_R$, where p_w is measured pressure, z_R is the vertical sensor location relative to a fixed datum, ρ is water density, and g is gravitational acceleration) and Darcy's law for laminar flow,

$$u = + \frac{K}{N} \frac{\partial(p_w/\rho g - z_R)}{\partial x} \quad (2)$$

$$w = - \frac{K}{N} \frac{\partial(p_w/\rho g - z_R)}{\partial z} \quad (3)$$

where z is vertical distance positive upward. Consistent with the model assumptions horizontal velocities are on average about 10 times larger than the vertical velocities (Figure 4). Vertical and horizontal velocities had similar magnitudes only during spring high tides when wave runup ran onto the beach above the watertable sensors, resulting in relatively large downward (negative) velocities on the rising tides and relatively large upward velocities as the watertable drained on the falling tides (Figure 4, Sep 24 to 31). However, 10-min-averaged vertical velocities were smaller than horizontal velocities 95% of the time. The vertical velocities corresponding to individual wave uprushes will be considered elsewhere.

Model-Data Comparisons

The model, driven with the observed 10-min-averaged shoreline location, predicts the observed watertable levels, except during and immediately after the two October storms (Figure 5). The fluctuations at the spring-neap frequency and the increased watertable fluctuations near the berm following the beach erosion on Oct 26 (Figure 1) are modeled qualitatively well. Consistent with previous results (Baird et al., 1998), breaking-wave-driven setup is important to the watertable fluctuations. Driving the model with the observed offshore water level fluctuations rather than the shoreline location results in underprediction of both the mean watertable levels and

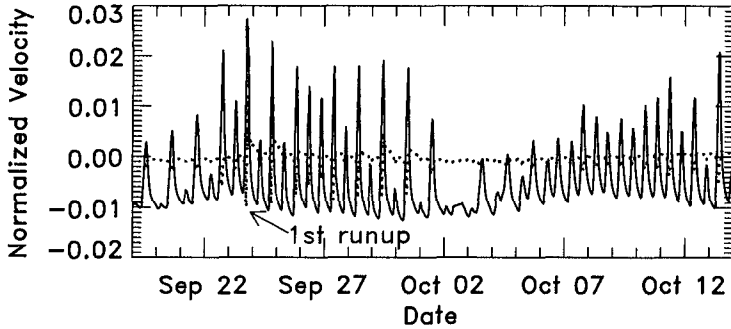


Figure 4: Normalized horizontal (u/K , solid curve) and vertical (w/K , dotted curve) velocities versus time. Velocities were estimated from 10-min averaged hydraulic heads measured with horizontally separated sensors at 39 and 53 m and vertically separated sensors at 46 m and elevations 0.6 and -2.2 m, respectively.

the fluctuation amplitudes, primarily because the shoreline is farther offshore when setup is not included (Figure 5).

The strong onshore decay and significant phase delays of diurnal, semi-diurnal, and higher frequency tidal watertable fluctuations are also predicted accurately (Figure 6). There is little energy at tidal harmonic frequencies in offshore tidal fluctuations (8 and 6 hr periods in Figure 3) and the increased energy in watertable fluctuations at these harmonics appears to be generated nonlinearly in the vicinity of the moving shoreline (Raubenheimer et al., in prep.). However, inland of the most onshore locations of the shoreline ($x \approx 35$ m), the watertable fluctuations are described well by solutions to the linearized Boussinesq equation, which have the form

$$\eta(x, t) = \eta_0 e^{-k_R x} \cos(\omega t - k_I x) \quad (4)$$

where η_0 is the shoreline fluctuation amplitude, ω is the frequency in radians, and k_R and k_I are the real and imaginary parts of the wavenumber, respectively, given by

$$k_R = k_I = \sqrt{\frac{N\omega}{2KD_{av}}} \quad (5)$$

where D_{av} is the average aquifer depth. Similar to observations, the linearized equation (4) predicts that the amplitudes decay exponentially, and the phase lags vary linearly with distance inland (Figure 6).

The Boussinesq model (1) does not predict the increase in the watertable elevation landward of the berm ($x > 50$ m) observed during the October storms

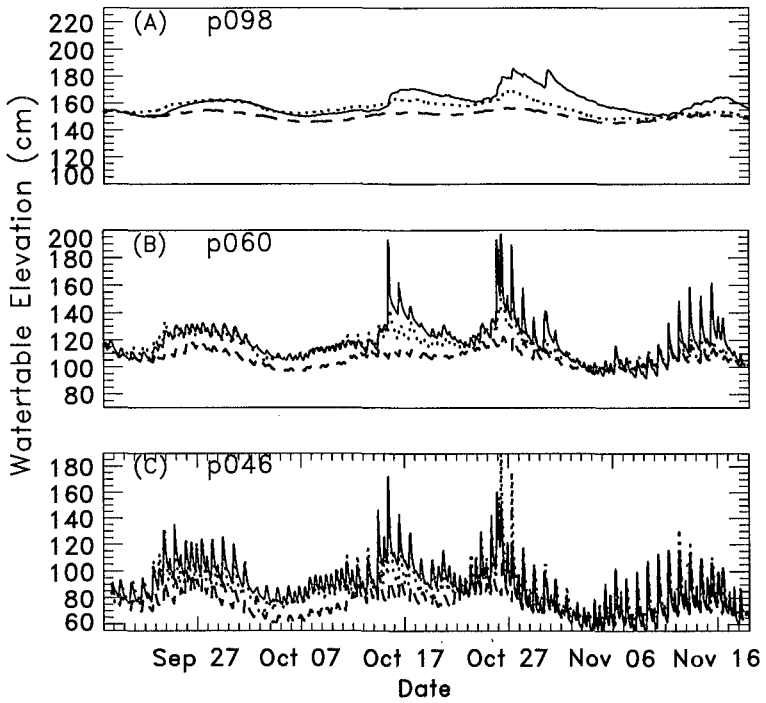


Figure 5: Watertable fluctuations observed (solid curves) and predicted by the numerical model (1) driven with the observed shoreline location (dotted curves) and offshore water level (dashed curves) versus time. Cross-shore distances are (A) 98, (B) 60, and (C) 46 m.

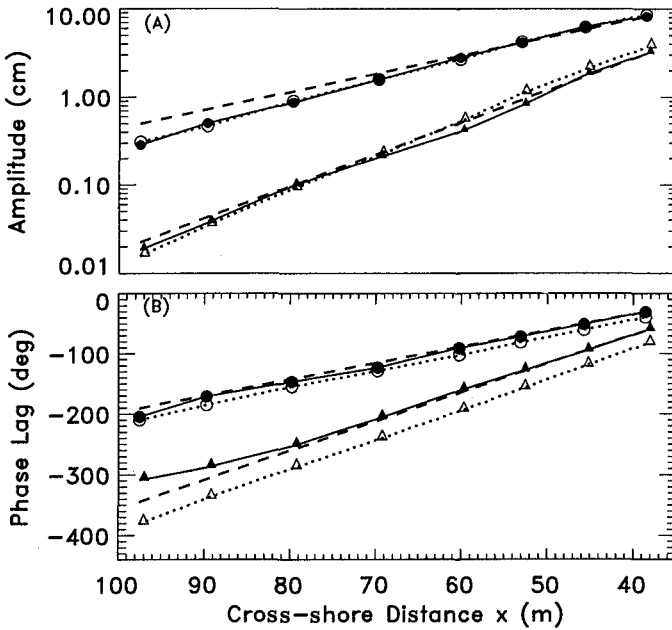


Figure 6: (A) Root-mean-square amplitudes and (B) phase lags relative to the shoreline for watertable fluctuations with periods of 25 (circles) and 8 hr (triangles) versus cross-shore distance inland from the mean shoreline location. Solid symbols with solid curves and open symbols with dotted curves are observed and predicted (with the nonlinear model) values, respectively, calculated from cross-spectra with 48 dof. Dashed lines represent linear theory predictions calculated using (4), (5), and observations at 39 m. Results for 6 and 12 hr periods are similar.

that coincided with spring tides (e.g., Figure 5, Oct 15 and 25). For the simplified case of no tides and monochromatic waves, the inland overheight of the watertable is independent of grain size and beach hydraulic conductivity (Kang et al., 1994). Using laboratory observations of watertable fluctuations owing to random breaking sea-swell waves, Kang et al. (1994) determined an empirical formula for $\bar{\eta}_w$, the time-averaged wave-driven overheight

$$\bar{\eta}_w = 0.62\sqrt{HL} \tan \beta_f \quad (6)$$

where H and L are the offshore significant wave height and wavelength, respectively, and β_f is the foreshore slope. The estimated (with (6)) wave-driven overheight ranges from 9 to 47 cm, but maxima of $\bar{\eta}_w$ do not coincide with the storm events during which offshore wave heights increased, but wavelengths ($L = gT^2/2\pi$) decreased (Figure 2B). Presumably, to predict the storm-induced watertable increases it is necessary to account for the effects of ponding water behind the berm (and the resulting infiltration) and the runup of (nonbreaking) infragravity waves. Differences between model predictions and observations may also result from neglecting the effects of the capillary fringe (e.g., Gillham, 1984; Li et al., 1997; Turner and Nielsen, 1997), trapped air within the watertable, and salinity (density) gradients (e.g., Nielsen, 1998). Despite the model simplifications and inaccuracies during the storms, model errors are small when the seaward boundary condition is given by the observed shoreline location (including setup). The 2 month average (and standard deviation) of differences between modeled and observed watertable levels are less than 6 ± 7 cm for all sensors landward of the maximum shoreline.

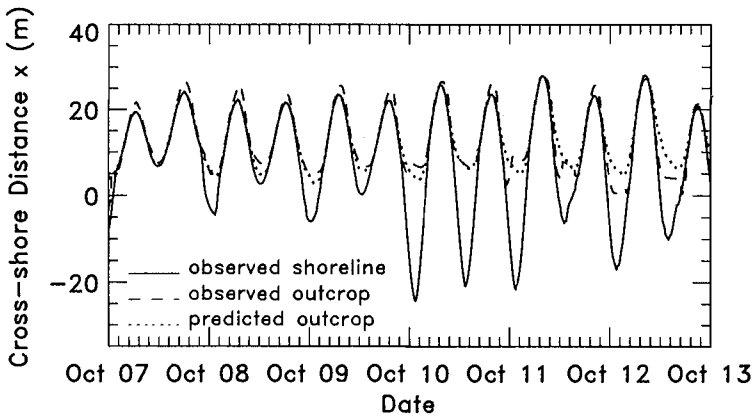


Figure 7: Cross-shore position of the 10-min averaged observed shoreline (solid curve) and observed and predicted watertable outcrop (dashed and dotted curves, respectively) versus time. The seepage face is located between the shoreline and the watertable outcrop.

When the tide falls more rapidly than the beach can drain, a seepage face forms between the watertable outcrop and the shoreline (Figure 7). The observed outcrop locations are predicted well by the nonlinear Boussinesq equation (1). Previous studies have suggested that the seepage face width on macrotidal beaches can be estimated assuming that the watertable outcrop position is independent of the pressure distribution within the beach, and depends only on the rate that the tide falls, the beach slope, and the value of K/N (Dracos, 1963; Turner, 1993). However reasonable agreement between the simple model of Dracos (1963) and the present outcrop observations is possible only if the ratio K/N is increased unrealistically (by a factor of 8) relative to that used in the numerical Boussinesq model.

Conclusions

Watertable levels observed for 2 months within a sandy beach depended on tidal levels, wind-waves and wave-driven setup, and the beach profile. Overtopping during spring high tides resulted in increased watertable levels for several days (Figure 2). Wind-waves of similar offshore height during neap tides had less effect on the watertable. Similar to previous observations, diurnal and semi-diurnal watertable fluctuations decreased inland (Figures 2, 3, 5, and 6). Although diurnal and semi-diurnal watertable fluctuations were damped almost completely 100 m inland of the mean shoreline location, fluctuations at spring-neap frequencies remained significant. Beach erosion during a storm resulted in larger tidal watertable fluctuations owing to the landward displacement of the shoreline. The observed horizontal flow in the watertable was usually much larger than the vertical flow (Figure 4), consistent with the assumptions in the nonlinear Boussinesq equation for watertable fluctuations in shallow aquifers.

The observed watertable levels (Figures 5 and 6) and seepage face width (Figure 7) are predicted accurately by a numerical model based on the nonlinear Boussinesq equation and driven with the observed 10-min averaged shoreline location (which includes wave-driven setup). When the model is driven with the offshore water levels (without setup), mean watertable levels and fluctuations are underpredicted. Watertable fluctuations (Figure 3) at harmonics of the tidal frequencies are nonlinearly generated near the moving shoreline location, but farther onshore the amplitudes and phases of watertable fluctuations are predicted well by solutions to the linearized Boussinesq equation (Figure 6).

Acknowledgements

This research was supported by the Office of Naval Research (Coastal Dynamics), the Naval Research Laboratory, the National Science Foundation, and the Mellon Foundation. Staff from the Center for Coastal Studies deployed and maintained the nearshore instruments. Offshore wave information was provided by the Coastal Data Information Program. The cooperation of the staff at Torrey Pines State Park is gratefully acknowledged.

References

- Baird, A.J., T. Mason, and D.P. Horn, Validation of a Boussinesq model of beach ground water behavior, *Marine Geol.*, submitted, 1998.
- Bouwer, H. and R.C. Rice, A slug test for determining hydraulic conductivity of unconfined aquifers with completely or partially penetrating wells, *Water Res. Res.*, 12, 423-428, 1976.
- Dracos, T., Ebene nichtstationare grundwasserabflüsse mit freier oberfläche, Swiss Federal Tech. Lab. Hydraul. Res. Soil Mech., Rep. 57, 114pp., 1963.
- Duncan, J.R., The effects of watertable and tide cycle on swash-backwash sediment distribution and beach profile development, *Marine Geol.*, 2, 186-197, 1964.
- Eliot, I.G., and D.J. Clarke, Semi-diurnal variation in beachface aggradation and degradation, *Marine Geol.*, 79, 1-22, 1988.
- Emery, K.O., and J.F. Foster, Watertables in marine beaches, *J. Marine Res.*, 7, 644-654, 1948.
- Gillham, R.W., The capillary fringe and its effect on watertable response, *J. Hydrol.*, 67, 307-324, 1984.
- Grant, U.S., Influence of the watertable on beach aggradation and degradation, *J. Marine Res.*, 7, 655-660, 1948.
- Harrison, W., C.S. Fang, and S.N. Wang, Groundwater flow in a sandy tidal beach. 1. One dimensional finite element analysis, *Water Res. Res.*, 7, 1313-1322, 1971.
- Kang, H.-Y., P. Nielsen, and D.J. Hanslow, Watertable overheight due to wave runup on a sandy beach, *Proc. 24th Int. Conf. Coastal Eng.*, Kobe, Japan, 1994.
- Kang, H.-Y., and P. Nielsen, Watertable dynamics in coastal areas, *Proc. 25th Int. Conf. Coastal Eng.*, Orlando, FL, 1996.
- Lanyon, J.A., I.G. Eliot, and D.J. Clarke, Groundwater variation during semi-diurnal spring tidal cycles on a sandy beach, *Austr. J. Marine Fresh. Res.*, 33, 377-400, 1982.
- Li, L., D.A. Barry, and C.B. Pattiaratchi, Numerical modeling of tide-induced beach water table fluctuations, *Coastal Eng.*, 30, 105-123, 1997a.
- Li, L., D.A. Barry, J.-Y. Parlange, and C.B. Pattiaratchi, Beach watertable fluctuations due to wave run-up: Capillarity effects, *Water Res. Res.*, 35, 935-945, 1997b.
- Liu, P.L.-F., and J. Wen, Nonlinear diffusive surface waves in porous media, *J. Fluid Mech.*, 347, 119-139, 1997.
- Nielsen, P., Tidal dynamics of the water table in beaches, *Water Res. Res.*, 26, 2127-2134, 1991.

Nielsen, P., R. Aseervatham, J.D. Fenton, and P. Perrochet, Groundwater waves in aquifers of intermediate depth, *Adv. Water Res.*, 20, 37-43, 1996.

Packwood, A.R., The influence of beach porosity on wave uprush and backwash, *Coastal Eng.*, 7, 29-40, 1983.

Raubenheimer, B., R.T. Guza, and S.L. Elgar, Tidal watertable fluctuations in a sandy ocean beach, in preparation, 1998.

Turner, I.L., Watertable outcropping on macrotidal beaches: a simulation model, *Marine Geol.*, 115, 227-238, 1993.

Turner, I.L., and P. Nielsen, Rapid water table fluctuations within the beach face: Implications for swash zone sediment mobility?, *Coastal Eng.*, 32, 45-59, 1997.

van Gent, M.R.A., The modeling of wave action on and in coastal structures, *Coastal Eng.*, 22, 311-339, 1994.

Waddell, E., Swash-groundwater-beach profile interactions, In: Davis, R.A. and R.L. Ethington (eds.), *Beach and Nearshore Sedimentation*, SEPM No. 24, 115-125., 1976.